Journal of Applied Fluid Mechanics, Vol. 18, No. 6, pp. 1459-1469, 2025.
Available online at www.jafmonline.net, ISSN 1735-3572, EISSN 1735-3645.
https://doi.org/10.47176/jafm.18.6.3227

Size Distribution and Mean Diameter of Microbubbles in Different Types of Ejector Bubble Generators

I. Catrawedarma[1†], S. Ton[2], D. Dwi Pranowo[3], and F. Surahmanto[4]

[1] *Department of Mechanical Engineering, Politeknik Negeri Banyuwangi, Jalan Raya Jember Km. 13, Kabat, Banyuwangi 68461, Indonesia*
[2] *Department of Agribusiness, Politeknik Negeri Banyuwangi, Jalan Raya Jember Km. 13, Kabat, Banyuwangi 68461, Indonesia*
[3] *Department of Civil Engineering, Politeknik Negeri Banyuwangi, Jalan Raya Jember Km. 13, Kabat, Banyuwangi 68461, Indonesia*
[4] *Department of Mechanical Engineering Education, Universitas Negeri Yogyakarta, Yogyakarta 55281, Indonesia*

†*Corresponding Author Email: ignb.catrawedarma@poliwangi.ac.id*

ABSTRACT

This study investigates the influence of air discharge on bubble size distribution across various types of bubble generators. Air discharge rates were adjusted between 0.1 lpm and 1.0 lpm for ejector, ejector-barrier plate, and venturi bubble generators, under a controlled experimental setup. High-speed camera footage captured bubble images, which were then analyzed to determine size distributions. A predictive correlation for bubble size distribution was formulated using the Buckingham Pi theorem. Results revealed that increased air discharge correlated with larger bubble diameters, with average increases of 8.01%, 10.71%, and 9.25% for ejector, ejector-barrier plate, and venturi generators, respectively. Notably, the ejector-barrier plate generator exhibited the greatest capability for producing smaller bubbles, with a peak increase in the probability density function of 13.95% for the ejector type, 18.05% for the ejector-barrier plate type, and 9.49% for the venturi type. Experimental findings aligned well with the proposed predictive model for average diameter and bubble size distribution.

Article History

Received October 31, 2024
Revised February 4, 2025
Accepted February 6, 2025
Available online March 30, 2025

Keywords:

Barrier plate
Air discharge
Image analysis
Log-normal distribution
Buckingham Phi theorem

1. INTRODUCTION

Micro-sized bubbles have significant potential in various applications due to their large contact area and ability to interact with other molecules (Huang et al., 2020a). Microbubbles are employed in wastewater treatment to reduce pollutants and fine particles during flotation processes (Khuntia et al., 2012; Liu et al., 2012), as well as in water and particle circulation through airlift pump systems (Ligus et al., 2019; Catrawedarma et al., 2020, 2021; Enany et al., 2021). Additionally, microbubbles are used for food decontamination, washing fresh produce, and inactivating microbes (Zhang & Tikekar, 2021; Lu et al., 2023). In agriculture and aquaculture, microbubbles enhance the growth rates of plants and fish (Bagatur, 2014; Lim et al., 2019a).

Various microbubble generators have been developed, including sonication and mechanical agitation methods (Xu et al., 2008), electrochemical methods (Wu et al., 2008), and hydrodynamic methods (Juwana et al., 2019; Mawarni et al., 2023). The hydrodynamic method is particularly versatile and involves modifications to channel shapes, such as the swirl type, which utilizes centrifugal force to increase shear force (Tabei et al., 2007; Terasaka et al., 2011; Mawarni et al., 2023), as well as orifice and spherical body types (Sadatomi et al., 2005, 2012), and venturi types (Gordiychuk et al., 2016; Afisna et al., 2017; Lim et al., 2019b). The orifice, spherical body, and venturi types rely on the throttling effect to increase flow velocity and shear force, breaking air into smaller bubbles.

The orifice type creates a sudden reduction in the channel cross-section at its center, while the spherical body type narrows the cross-section toward the channel edge. Both designs result in higher energy loss compared to the venturi type, which gradually reduces the channel's cross-section to enhance flow velocity. The venturi type is also easier to maintain due to its simple structure and absence of moving parts, making it more economical with lower energy losses (Basso et al., 2018; Huang et al., 2020b).

Researchers have optimized the venturi type to achieve smaller bubble size distributions and reduced energy consumption. Innovations include the addition of a porous

NOMENCLATURE

d	nozzle diameter	U_G	air velocity
d_b	average bubble diameter	We_L	Weber number
D	water inlet diameter	ρ_L	water density
D_G	air inlet diameter	ρ_G	air density
M	mean of the natural logarithmic microbubble diameter	μ_L	water viscosity
Q_G	gas volume flow rate	σ_L	water surface tension
Q_L	liquid volume flow rate	χ^2	Lockhart Martinelli parameter
Re	Reynolds number	MAPE	Mean Absolute Percentage Error
R_o	circularity	PDF	Probability Density Function
S	standard deviation of the natural logarithmic microbubble diameter	RGB	Red Green Blue
U_L	water velocity		

pipe to the air inlet to minimize bubble size (Yoon, 1993; Liu et al., 2012, 2013; Deendarlianto et al., 2017; Afisna et al., 2017; Juwana et al., 2019) and investigations into the effects of air and water discharges, throat diameter, and nozzle angle (Sun et al., 2017; Zhao et al., 2017; Huang et al., 2020b). Experimental results show that maintaining constant water discharge, throat diameter, and nozzle angle results in smaller average bubble diameters at lower air discharges. While the diameter and number of air inlet channels appear to have minimal impact on bubble size (Li et al., 2017; Lee et al., 2019). Baylar et al. (2010) reported that the air hole diameter significantly influences bubble diameter and quantity. Ding et al. (2021) developed a two-stage venturi bubble generator to produce microbubbles with smaller diameters. The development of ejector bubble generators has been carried out by various researchers such as (Lim et al., 2019b) designing an ejector bubble generator with water as a horizontal driving fluid for waste water treatment and also used in nitrification and denitrification processes (Lim et al., 2019a). Some researchers (Park & Yang, 2017; Seo et al., 2018) made an ejector bubble generator where water flows vertically and air flows horizontally. Sari et al. (2024) looked at the outlet pressure of the horizontal ejector bubble generator using a probability density function and a power spectrum density.

Theoretical models for predicting bubble diameter often rely on dimensional analysis. For example, Yin et al. (2015) proposed a correlation as a function of the Weber number, gas volume ratio, Reynolds number, and surface tension. Gordiychuk et al. (2016) developed a model based on the water Reynolds number, air Reynolds number, and air-water discharge ratio. Similarly, Juwana et al. (2019) presented an empirical model incorporating the air/water discharge ratio, air Reynolds number, and air Weber number. All these correlations emphasize the Reynolds number, as fluid discharge significantly affects it. However, none explicitly account for the Lockhart-Martinelli parameters, critical for two-phase flow interactions.

The literature review highlights that researchers have focused on individual bubble generator types, and varying geometric and operational parameters, yet discrepancies remain regarding the effects of air input diameter and quantity on microbubble formation. This study examines the influence of air discharge across various venturi bubble generator types, including ejector, ejector-barrier plate, and conventional venturi designs. The analysis begins with visual observations of bubble distributions in photographic images, followed by quantitative measurements using image processing methods. A new correlation is proposed, incorporating experimental data to predict bubble size while accounting for the Lockhart-Martinelli parameter's impact.

2. APPARATUS, PROCEDURE, AND METHODS

The schematic diagram of the apparatus utilized in the present study is shown in Fig. 1(a). The apparatus was designed at the Mechanical Engineering Workshop of Politeknik Negeri Banyuwangi, with its primary component being a transparent test pool measuring 100 cm in length, 50 cm in width, and 50 cm in height. A Sony ZV-1 high-speed camera, featuring 1000 fps, a 1/12800 shutter speed, an f/8.0 aperture, and an ISO setting of 4000, was employed to record the bubble flow videos. The study used three types of bubble generators—ejector, ejector-barrier plate, and venturi—whose dimensions are detailed in Figs 2(a), 2(b), and 2(c), respectively. The water input and output diameters for all bubble generator types were standardized at D=7 mm, while the nozzle diameter was d=2.33 mm. An aerator with 2.2 Watt power and a maximum output of 3.0 lpm was used to inject air to the bubble generator. A water pump with 12 Volt, 5 Ampere direct current, 100 psi, and a maximum of 5.0 lpm was conducted to supply pressurized water to the bubble generator.

The data collection process commenced by filling the test pool with tap water to a height of 45 cm. The bubble generator was positioned 5 cm above the pool bottom and centered along the pool width. A series of 50W LED lamps with a diffuse layer were installed behind the test pool to ensure uniform illumination, as depicted in Fig. 1(b). The camera was positioned 25 cm from the observation area directly in front of the bubble generator outlet. A ruler was placed in the observation area to establish a focus point and convert distance measurements from centimeters to pixels. A background image was captured while ensuring the water in the test pool remained static, facilitating the distinction between moving and stationary parts during image processing. The pump was then activated to deliver pressurized water to the bubble generator at maximum

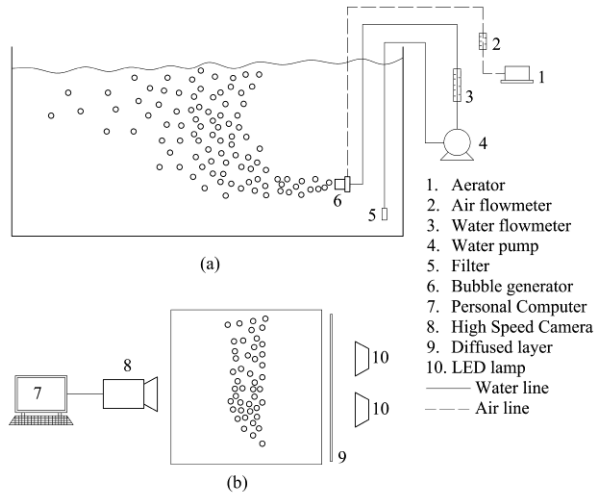

Fig. 1 (a) Apparatus schematic, (b) Image capturing schematic

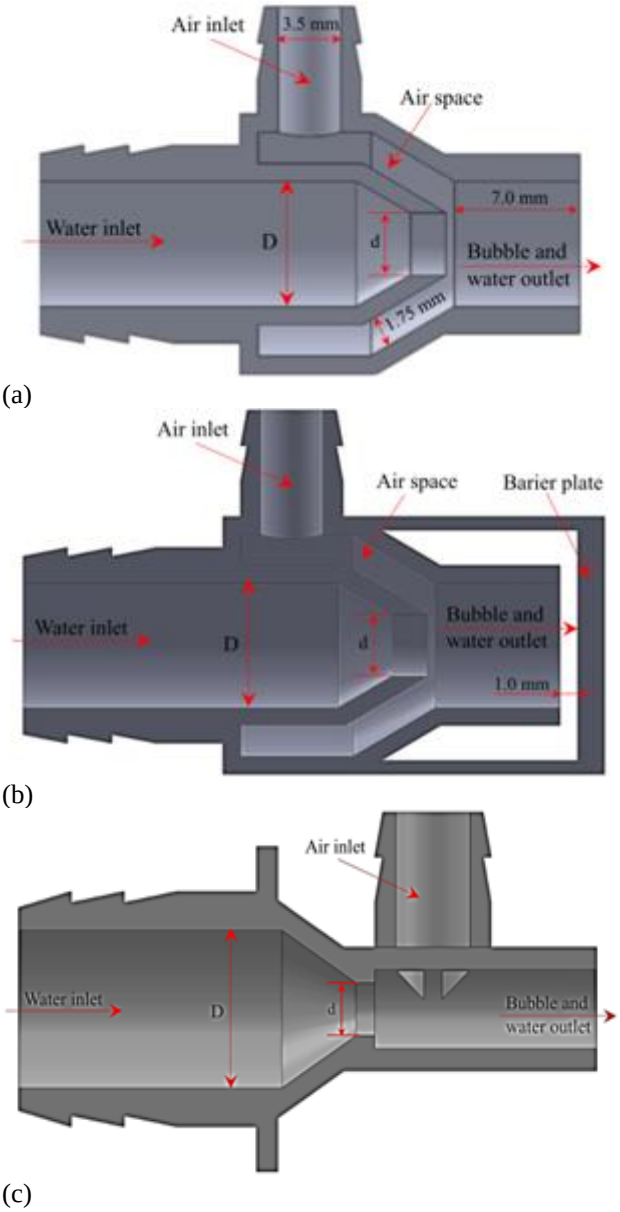

Fig. 2 Section view: (a) Ejector bubble generator type, (b) Ejector-barrier plate bubble generator type, (c) Venturi bubble generator type

discharge, as measured by a water flow meter with 2.5% accuracy. Subsequently, air was introduced from the aerator to the bubble generator, with discharges varying between 0.1 lpm and 1.0 lpm by using air flow meter with 3.0% accuracy. The mixture of water and air formed bubbles that exited through the outlet and dispersed into the pool. The bubble flow was recorded using the high-speed camera, and the footage was processed using image processing tools in the MATLAB commercial toolbox to measure bubble diameters.

The image processing procedure began with loading the image using the "imread" toolbox and converting the RGB image to grayscale with the "rgb2gray" command. The "imcrop" command was used to crop a uniformly lit section of the image, producing results shown in Fig. 3(a). Background subtraction was performed by subtracting the background image from the original image, distinguishing moving elements from static ones. Image quality was enhanced and filtered using the "imtophat," "imbothat," and "medfilt" commands. The processed image was then converted to a binary format using the "im2bw" command, with the threshold adjusted to produce the optimal binary image, as shown in Fig. 3(b). White and black areas were inverted using the "imcomplement" command, and gaps were filled using the "imfill" command. Separation of objects using the circularity value (R_0) into objects with $R_0 > 1$, as in Fig. 3(c), and objects with $R_0 \leq 1$, as in Fig. 3(d). The equation for calculating the Ro value is as follows:

$$R_O = S.(4\pi A)^{(-1/2)} \tag{1}$$

where S represents the object's perimeter and A its area. Objects with $R_0 > 1$underwent further processing using the watershed method, as illustrated in Fig. 3(e). The resulting watershed image was merged with images containing $R_0 \leq 1$, as shown in Fig. 3(f). Finally, the centroid coordinates and radius of each object were identified, creating a red circular outline for each object, as shown in Fig. 3(g). Diameter data for each object was stored in a .xls file for subsequent analysis of bubble size distribution.

3. RESULTS AND DISCUSSION

3.1 Bubble Size Distribution

Figure 4 provides a visual representation of the bubbles produced by the three types of microbubble generators at Qg = 0.3 lpm. Figure 4(a) illustrates the bubble size distribution for the ejector bubble generator without a barrier plate. A significant variation in bubble sizes, ranging from large to small, is observed. Bubbles exiting the ejector come into direct contact with the surrounding water, resulting in bubble distribution and structure influenced solely by the hydrostatic pressure of the water. As the hydrostatic pressure increases, the size and quantity of the bubbles decrease. The hydrodynamic force of water, which disrupts the bubble's surface tension, closely relates to hydrostatic pressure. If the hydrodynamic force of water is greater than the surface tension of the bubble, it will burst into several bubbles of smaller sizes.

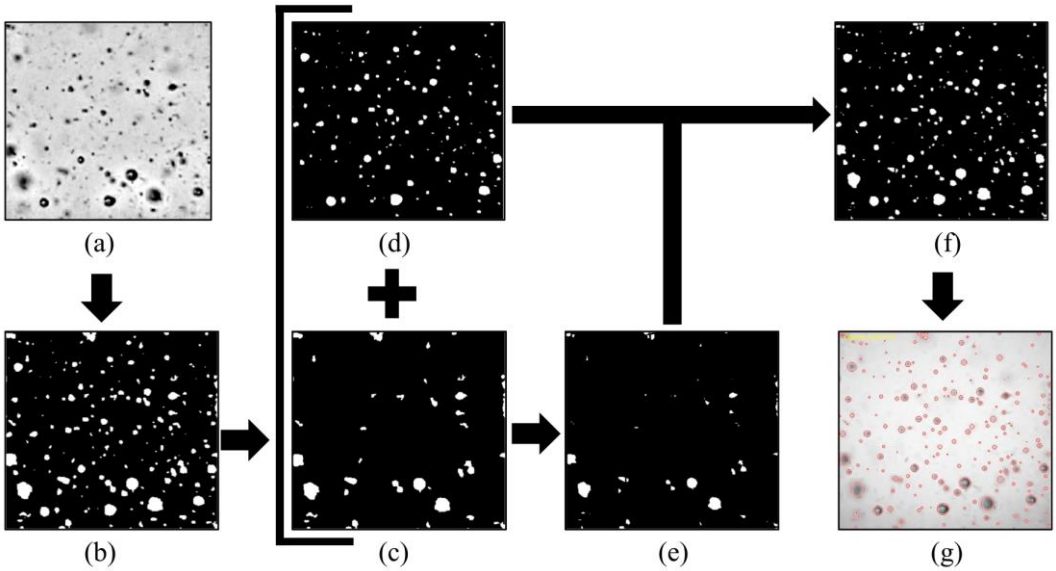

Fig. 3 Image processing step: (a) Original image, (b) Binary image, (c) Objects with high Ro, (d) Objects with low Ro, (e) Watershed object, (f) Merged image (low Ro+Watershed), (g) Circle overlaid on the original image

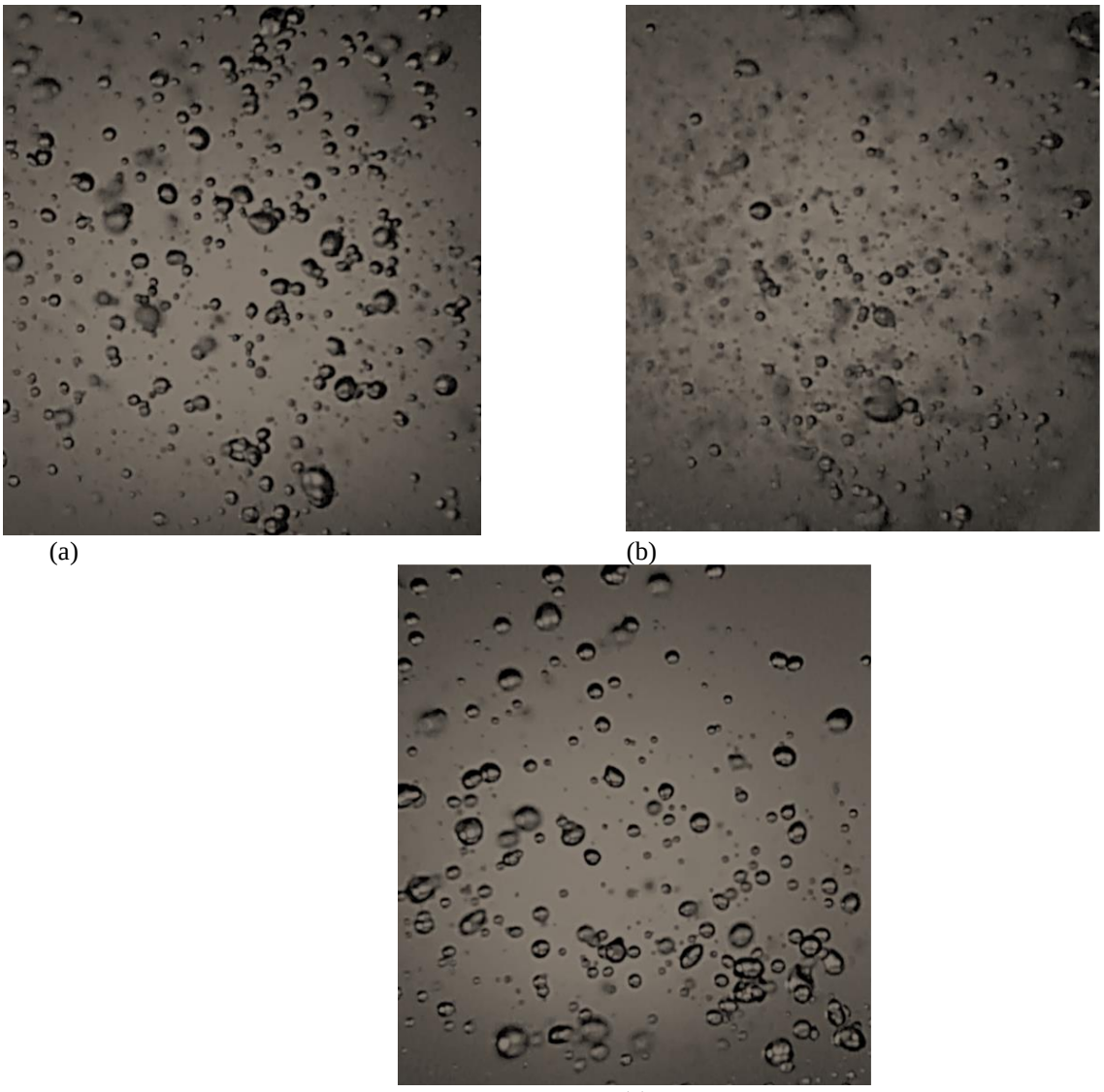

Fig. 4 Visual observation at Qg = 0.3 lpm of: (a) Ejector bubble generator type, (b) Ejector-barier plate bubble generator type, (c) Venturi bubble generator type

Figure 4(b) shows the bubble size distribution for the ejector type equipped with a barrier plate at the outlet. The ejector-barrier plate configuration produces smaller and more numerous bubbles compared to the ejector without a barrier plate. This occurs due to the collision of bubbles with the barrier plate positioned at the outlet, which alters the flow velocity field and increases flow momentum. The enhanced flow momentum generates greater shear forces on the bubble surfaces, causing them to fragment into smaller sizes. Shear force is one of the external forces that disrupts the bubble interface, causing interface instability. If the shear force is greater and exceeds the bubble surface tension, the bubble will burst into smaller bubbles.

The fragmented bubbles flow upward through the gap between the outlet and the barrier plate. Unlike the ejector without a barrier plate, the bubble-water mixture produced by this configuration does not significantly displace the surrounding water. In contrast, bubbles released from the ejector without a barrier plate are propelled further from the outlet, with the accompanying water movement increasing hydrodynamic force. Figure 4(c) presents a visual observation of bubbles generated by the venturi microbubble generator. The number of bubbles produced by this configuration is notably fewer than those produced by the previous two types. This observation is supported by the air space within the ejector configuration, which enables a higher bubble generation capacity. In the venturi type, air occupies the low-pressure region in the throat, leading to increased air suction and a reduced number of bubbles being produced.

Figure 5 illustrates the bubble size distribution for all types of bubble generators under varying air discharges. Across all generator types, it is observed that higher input air discharges reduce the likelihood of forming smaller bubbles. This trend is evident from the peak probability values, which increase as air discharge decreases. Furthermore, the curves demonstrate that smaller air discharges yield higher kurtosis values, indicating a narrower and more uniform distribution of bubble sizes, particularly in the diameter range below 100 µm. The bubble diameter above 100 µm is getting smaller in frequency of occurrence, or the number of bubbles larger than 100 µm is very little, produced by the three bubble generators, so that the chance of occurrence is getting smaller. This is a transition point from an area with a high probability distribution to an area with a lower probability distribution.

At an air discharge of Qg=0.1 lpm, the probability of forming bubbles smaller than 60 µm is the highest. Conversely, higher air discharges result in larger bubble sizes due to the increased air fraction, which promotes the formation of larger bubbles. With greater bubble volumes, the inertial force is more significant, aiding the bubbles in maintaining their structure. For all bubble generator types, an increase in air flow rate correlates with a rise in bubble diameter, with average increases of 8.01%, 10.71%, and 9.25% for the ejector, ejector-barrier plate, and venturi bubble generators, respectively.

The ejector-barrier plate generator achieves a maximum probability of 0.015 at Qg=0.1 lpm, as shown in Figure 5(b),

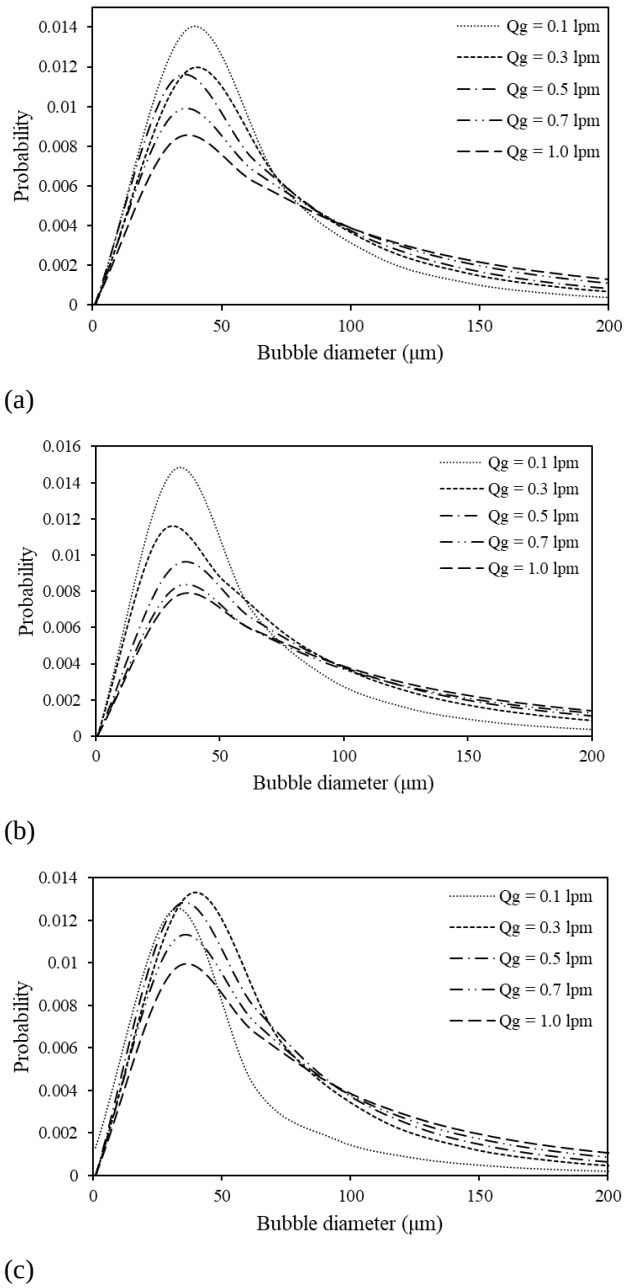

Fig. 5 Bubble size distribution: (a) Ejector bubble generator type, (b) Ejector-barrier plate bubble generator type, (c) Venturi bubble generator type

followed by the ejector generator with a maximum probability of 0.014 (Fig. 5(a)), and the venturi generator at 0.013 in Fig. 5(c). These values indicate that the ejector-barrier plate generator is the most effective at producing bubbles smaller than 100 µm. This efficiency is attributed to the interaction between the bubbles and the barrier plate, which enhances momentum and shear stress, causing the bubbles to fragment into smaller sizes. In contrast, bubble generators without a barrier plate, such as the ejector and venturi types, rely solely on momentum changes and hydrostatic pressure to disrupt the outgoing bubbles, resulting in a lower likelihood of producing bubbles smaller than 100 µm. A decrease in air discharge enhances the formation of microbubbles, with the peak

Table 1 Variables Influencing Bubble Diameter

No	Variable	Sym	Unit	Dimension		
				M	L	T
1	Average bubble diameter	d_b	m		1	
2	Water velocity	U_L	m/s		1	-1
3	Air velocity	U_G	m/s		1	-1
4	Water density	ρ_L	kg/m^3	1	-3	
5	Air density	ρ_G	kg/m^3	1	-3	
6	Water viscosity	μ_L	kg/m.s	1	-1	-1
7	Water surface tension	σ_L	kg/s^2	1		-2
8	Air inlet diameter	D_G	m	1		
9	Water inlet diameter	D	m	1		
10	Nozzle diameter	d	m	1		

probability density function (PDF) increasing by 13.95% for the ejector type, 18.05% for the ejector-barrier plate type, and 9.49% for the venturi type.

3.2 Dimensional Analysis of Bubble Diameter

Dimensional analysis was employed to develop correlations for determining the average bubble diameter. This method establishes relationships among variables influencing bubble size, as summarized in Table 1.

Using the Buckingham Pi theorem, U_L, ρ_L, D were selected as the repeated variables. From the chosen variables, seven dimensionless parameters were derived as follows:

$$\Pi_1 = \frac{d_b}{D} \tag{2}$$

$$\Pi_2 = \frac{U_G}{U_L} \tag{3}$$

$$\Pi_3 = \frac{\rho_G}{\rho_L} \tag{4}$$

$$\Pi_4 = \frac{\mu_L}{U_L . \rho_L . D} \tag{5}$$

$$\Pi_5 = \frac{\sigma_L}{U_L^2 . \rho_L . D} \tag{6}$$

$$\Pi_6 = \frac{D_G}{D} \tag{7}$$

$$\Pi_7 = \frac{d}{D} \tag{8}$$

These dimensionless parameters can be consolidated into a single phi parameter for greater interpretability:

$$\Pi_8 = \Pi_8 . \Pi_6^2 = \frac{U_G}{U_L}\left(\frac{D_G}{D}\right)^2 \tag{9}$$

$$\Pi_9 = \frac{1}{\Pi_3}.\left(\frac{1}{\Pi_2}\right)^2 = \frac{\rho_L}{\rho_G}\left(\frac{U_L}{U_G}\right)^2 \tag{10}$$

The functional relationship involving all phi parameters can be expressed as:

$$\Pi_1 = f\left(\Pi_4, \Pi_5, \Pi_7, \Pi_8, \Pi_9\right) \tag{11}$$

$$\frac{d_b}{D} = f\left(\frac{\mu_L}{U_L . \rho_L . D}, \frac{\sigma_L}{U_L^2 . \rho_L . D}, \frac{d}{D}, \frac{U_G}{U_L}\left(\frac{D_G}{D}\right)^2, \frac{\rho_L}{\rho_G}\left(\frac{U_L}{U_G}\right)^2\right) \tag{12}$$

When decomposed, each component is represented as follows, with respective coefficients:

$$\frac{d_b}{D} = a\left(\frac{\mu_L}{U_L . \rho_L . D}\right)^b \left(\frac{\sigma_L}{U_L^2 . \rho_L . D}\right)^c \left(\frac{d}{D}\right)^d \left(\frac{U_G}{U_L}\left(\frac{D_G}{D}\right)^2\right)^e \left(\frac{\rho_L}{\rho_G}\left(\frac{U_L}{U_G}\right)^2\right)^f \tag{13}$$

With:

$$\frac{\mu_L}{U_L . \rho_L . D} = \frac{1}{\mathrm{Re}_L} \tag{14}$$

$$\frac{\sigma_L}{U_L^2 . \rho_L . D} = \frac{1}{We_L} \tag{15}$$

$$\frac{U_G}{U_L}\left(\frac{D_G}{D}\right)^2 = \frac{Q_G}{Q_L} \tag{16}$$

$$\frac{\rho_L}{\rho_G}\left(\frac{U_L}{U_G}\right)^2 = \chi^2 \tag{17}$$

Where Re_L represents the liquid Reynolds number, We_L denotes the liquid Weber number, $\frac{Q_G}{Q_L}$ is the air-to-water flow rate ratio, and χ^2 refers to the Martinelli parameter.

In the current study, $\left(\frac{\mu_L}{U_L.\rho_L.D}\right)$, $\left(\frac{\sigma_L}{U_L^2.\rho_L.D}\right)$, and $\left(\frac{d}{D}\right)$ were maintained as constants, resulting in a general equation for calculating the bubble diameter ratio:

$$\frac{d_b}{D} = a\left(\frac{Q_G}{Q_L}\right)^b \left(\chi^2\right)^c \tag{18}$$

The coefficients a, b, and c were determined using nonlinear regression to fit the experimental data. Consequently, the empirical equations for the ratio of bubble diameter to inlet pipe diameter for the three types of bubble generators are:

$$\frac{d_b}{D} = 0.027\left(\frac{Q_G}{Q_L}\right)^{0.413} \left(\chi^2\right)^{0.038} \tag{19}$$

$$\frac{d_b}{D} = 0.031\left(\frac{Q_G}{Q_L}\right)^{0.413} \left(\chi^2\right)^{0.038} \tag{20}$$

$$\frac{d_b}{D} = 0.022\left(\frac{Q_G}{Q_L}\right)^{0.413} \left(\chi^2\right)^{0.038} \tag{21}$$

Equations (19), (20), and (21) represent the bubble diameter-to-inlet pipe diameter ratios for the ejector, ejector-barrier, and venturi-type bubble generators, respectively. Among these correlations, the coefficient a is smallest for the venturi-type bubble generator and largest for the ejector-barrier plate type. This difference suggests that the ejector-barrier plate type experiences the highest head loss, likely due to the additional air space and barrier plates, which increase flow friction. Additionally, the correlations reveal that the air-to-water discharge ratio significantly impacts the diameter of the bubbles formed, as indicated by its exponent of 0.413. This finding implies that higher air discharge results in larger average bubble diameters, while lower air discharge leads to smaller bubbles. This behavior is attributed to the deceleration of air supplied in the divergent region of the bubble generator at higher air discharges, which increases the void fraction. The resulting bubbles tend to cluster and coalesce, forming larger bubbles (Zhao et al., 2018, 2019).

The Martinelli parameter is defined as the ratio of the liquid to gas Froude number, where the Froude number represents the ratio of inertial forces to gravitational effects. With gravitational effects constant, the Froude number is predominantly influenced by inertial forces, which are strongly affected by fluid velocity. Higher liquid velocities result in smaller average bubble diameters due to increased flow velocity and momentum changes, which enhance turbulence. This heightened turbulence increases the shear forces at the bubble interface, causing the bubbles to fragment into smaller sizes.

Figure 6 compares the average bubble diameters predicted by the proposed model with experimental data, alongside comparisons to the models proposed by Juwana et al. (2019) and Gordiychuk et al. (2016). The current proposed model correlates very well with the experimental data. All of the experimental data is within the 10% error range and the mean absolute percentage error (MAPE) is 4.58%, 6.07%, and 3.02% for ejector, ejector-barrier plate, and venturi types, respectively. The proposed model aligns well with the experimental data, with all measurements falling within a 10% error margin. In contrast, the models by Juwana et al. (2019) and Gordiychuk et al. (2016) are applicable only up to db/D=0.015 as their predictions deviate beyond this range. The model by Juwana et al. (2019) and Gordiychuk et al. (2016) are not suitable for application at db/D values > 0.015. The MAPEs of the (Juwana et al., 2019) model are 10.07%, 18.46% and 12.71% for ejector, ejector barrier plate, and venturi types, respectively. The MAPEs of the (Gordiychuk et al., 2016) model are 14.50%, 21.61% and 8.28% for ejector, ejector barrier plate, and venturi types, respectively.

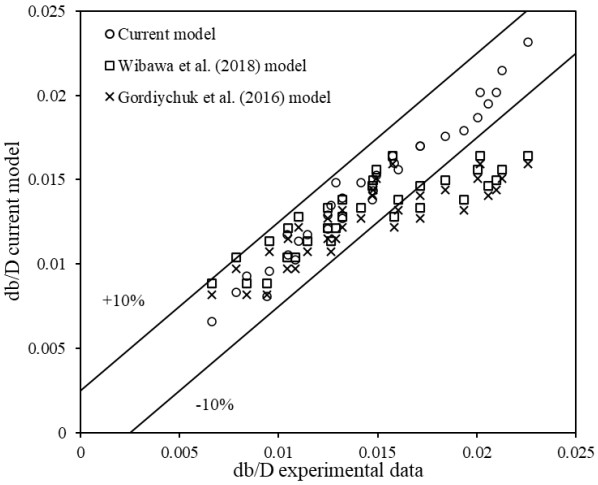

Fig. 6 Comparison Between the Proposed Model and Experimental Data

The model by Juwana et al. (2019) incorporates the air-to-water discharge ratio, the water Reynolds number, and the water Weber number, whereas the model by Gordiychuk et al. (2016) is based on the air-to-water discharge ratio, the water Reynolds number, and the air Reynolds number. However, when water discharge is held constant, both the water Reynolds number and the water Weber number remain relatively unchanged, as they are functions of water velocity. To address these limitations, a new model is proposed that incorporates the air-to-water discharge ratio and the Lockhart-Martinelli parameter. This approach accounts for the water Reynolds number, air Reynolds number, and water Weber number more comprehensively.

In certain applications, such as wastewater treatment (Gordiychuk et al., 2016) the bubble size distribution is more relevant than the average bubble diameter. To predict bubble size distribution, a log-normal distribution is employed, expressed by the following equation:

$$P(x) = \frac{1}{xS\sqrt{2\pi}} e^{\left(\frac{-(\ln x - M)^2}{2S^2}\right)} \quad (22)$$

Here, x represents the bubble diameter, $P(x)$ denotes the probability density, and M and S are the mean and standard deviation of the natural logarithm of the microbubble diameter, respectively.

Using the dimensional analysis approach, an empirical equation for the log-normal distribution parameters can be developed as a function of the discharge ratio and Martinelli parameters. This relationship is expressed as:

$$(M,S) = a\left(\frac{Q_G}{Q_L}\right)^b \left(\chi^2\right)^c \quad (23)$$

The coefficients a, b, and c are determined through nonlinear regression to fit the experimental data for each M and S parameter. The results are summarized in Table 2.

Table 2 reveals that all log-normal parameters have a Mean Absolute Percentage Error (MAPE) of less than 10% when compared with experimental data. If the correlation coefficients b, and c remain constant across all bubble generator types, the coefficient a serves as a distinguishing indicator for the different generator types. Notably, the ejector-barrier plate type exhibits the highest values for both M and S, suggesting that this generator type produces the broadest microbubble distribution.

When compared to an error threshold of 5%, all coefficients for the M parameter fall within this limit, as depicted in Fig. 7(a). For the S, parameter, two data points fall outside the 10% error threshold, as shown in Fig. 7(b). These outliers correspond to the venturi bubble generator type at air flow rates of 0.1 lpm and 0.2 lpm. This deviation is likely due to the structural differences of the venturi generator, particularly the absence of air space, distinguishing it from the ejector type.

4. SUMMARY REMARKS

Research on bubble size distribution for various types of bubble generators has been conducted using image processing. A new correlation was also proposed through dimensional analysis using the Buckingham Pi theorem. The results are summarized as follows:

1. For all types of bubble generators, it was found that an increasing air flow rate resulted in larger bubble diameters, with average increases of 8.01%, 10.71%, and 9.25% for the ejector, ejector-barrier plate, and venturi bubble generator types, respectively.
2. Lower air discharge increases the probability of microbubble formation, with peak PDF increases of 13.95% for the ejector type, 18.05% for the ejector-barrier plate type, and 9.49% for the venturi type.
3. A correlation, defined as a function of the air-water flow rate ratio and the Lockhart-Martinelli parameters, was proposed to predict the average bubble diameter. This correlation aligns closely with experimental data,

Table 2 Log-Normal Parameters for Various Bubble Generator Types

Bubble generator type	Log-normal parameter	Correlation coefficient			MAPE (%)
		a	b	c	
Ejector	*M*	2.727	0.408	0.178	0.977
	S	0.913	0.300	0.088	1.403
Ejector-barier plate	*M*	2.795	0.408	0.178	1.759
	S	0.985	0.300	0.088	1.707
Venturi	*M*	2.63	0.408	0.178	3.471
	S	0.892	0.300	0.088	7.699

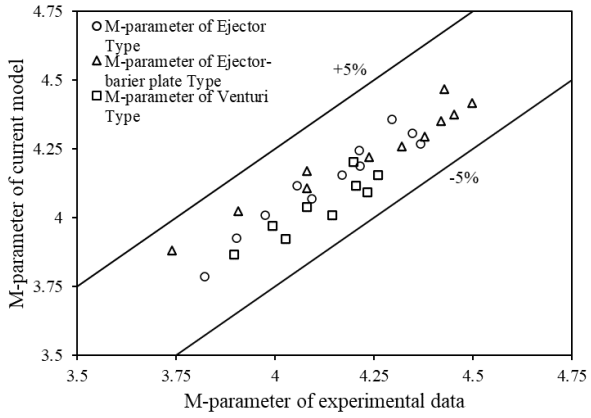

(a)

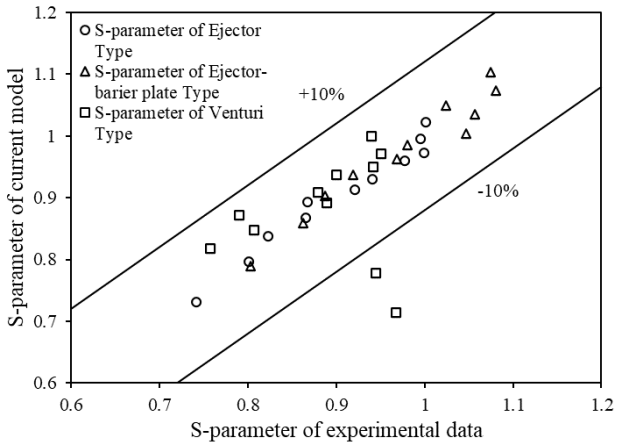

(b)

Fig. 7 Comparison of Log-normal distribution: (A) The *M* parameter, (B) The *S* parameter

with coefficients "*a*" of 0.027, 0.031, and 0.022 for the ejector, ejector-barrier plate, and venturi-type bubble generators, respectively.

4. Bubble size distribution can be approximated by a log-normal distribution, with maximum M and S parameters of 2.795 and 0.985, respectively, for the ejector-barrier plate type bubble generator.

ACKNOWLEDGMENT

The Badan Riset dan Inovasi Nasional funded this project through the Riset dan Inovasi untuk Indonesia Maju Gelombang IV (RIIM-4) scheme under contract No. 136/IV/KS/11/2023. The authors would like to express their profound appreciation for the financial support.

CONFLICT OF INTEREST

The authors declare that they have no known competing financial interests or personal relationships that could have influenced the work reported in this paper.

AUTHORS CONTIBUTION

IGNB. Catrawedarma: Conceptualization, Methodology, Investigation, Data curation, Formal analysis, Writing - original draft. **Sefri Ton:** Formal analysis, Validation, Review & Editing, Funding acquisition. **Dadang Dwi Pranowo:** Writing - Review & Editing, Resources, Funding acquisition. **Fredy Surahmanto:** Supervision, Review & Editing final draft.

REFERENCES

Afisna, L. P., Juwana, W. E., Indarto, I., Deendarlianto, D., & Nugroho, F. M. (2017). Performance of Porous-Venturi Microbubble Generator for Aeration Process. *Journal of Energy, Mechanical, Material, and Manufacturing Engineering*, *2*(2), 73–80. https://doi.org/10.22219/jemmme.v2i2.5054

Bagatur, T. (2014). Evaluation of plant growth with aerated irrigation water using venturi pipe part. *Arabian Journal for Science and Engineering*, *39*(4), 2525–2533. https://doi.org/10.1007/s13369-013-0895-4

Basso, A., Hamad, F. A., & Ganesan, P. (2018). Effects of the geometrical configuration of air–water mixer on the size and distribution of microbubbles in aeration systems. *Asia-Pacific Journal of Chemical Engineering*, *13*(6), e2259. https://doi.org/10.1002/apj.2259

Baylar, A., Ozkan, F., & Unsal, M. (2010). *Using Venturi Tubes in Two-Phase Aeration Processes.* Editörler: Mehmet Emin AYDIN. July 2021.

Catrawedarma, I., Deendarlianto, & Indarto. (2020). The performance of airlift pump for the solid particles lifting during the transportation of gas-liquid-solid three-phase flow: A comprehensive research review. *Proc IMechE Part E: J. Process Mechanical Engineering*, *0*(0), 1–23. https://doi.org/10.1177/0954408920951728

Catrawedarma, IGNB., Deendarlianto, & Indarto. (2021). Statistical characterization of flow structure of air – water two-phase flow in airlift pump – Bubble generator system. *International Journal of Multiphase Flow*, *138*(103596), 1–16. https://doi.org/10.1016/j.ijmultiphaseflow.2021.103596

Deendarlianto, D., Indarto, I., Juwana, W. E., Afisna, L. P., & Nugroho, F. M. (2017). Performance of porous-venturi microbubble generator for aeration process. *Journal of Energy, Mechanical, Material and Manufacturing Engineering*, *2*(2). https://doi.org/10.22219/jemmme.v2i2.5054

Ding, G., Li, Z., Chen, J., & Cai, X. (2021). An investigation on the bubble transportation of a two-stage series venturi bubble generator. *Chemical Engineering Research and Design*, *174*, 345–356. https://doi.org/10.1016/j.cherd.2021.08.022

Enany, P., Shevchenko, O., & Drebenstedt, C. (2021). Experimental evaluation of airlift performance for vertical pumping of water in underground mines. *Mine Water and the Environment*, *40*(4), 970–979. https://doi.org/10.1007/s10230-021-00807-w

Gordiychuk, A., Svanera, M., Benini, S., & Poesio, P. (2016). Size distribution and Sauter mean diameter of micro bubbles for a Venturi type bubble generator. *Experimental Thermal and Fluid Science*, *70*, 51–60. https://doi.org/10.1016/j.expthermflusci.2015.08.014

Huang, J., Sun, L., Du, M., Liang, Z., Mo, Z., Tang, J., & Xie, G. (2020a). An investigation on the performance of a micro-scale Venturi bubble generator. *Chemical Engineering Journal*, *386*, 120980. https://doi.org/10.1016/j.cej.2019.02.068

Huang, J., Sun, L., Liu, H., Mo, Z., Tang, J., Xie, G., & Du, M. (2020b). A review on bubble generation and transportation in Venturi-type bubble generators. *Experimental and Computational Multiphase Flow*, *2*(3), 123–134. https://doi.org/10.1007/s42757-019-0049-3

Juwana, W. E., Widyatama, A., Dinaryanto, O., Budhijanto, W., Indarto, & Deendarlianto. (2019). Hydrodynamic characteristics of the microbubble dissolution in liquid using orifice type microbubble generator. *Chemical Engineering Research and Design*, *141*, 436–448. https://doi.org/10.1016/j.cherd.2018.11.017

Khuntia, S., Majumder, S. K., & Ghosh, P. (2012). Microbubble-aided water and wastewater purification: A review. *Reviews in Chemical Engineering*, *28*(4–6). https://doi.org/10.1515/revce-2012-0007

Lee, C. H., Choi, H., Jerng, D. W., Kim, D. E., Wongwises, S., & Ahn, H. S. (2019). Experimental investigation of microbubble generation in the venturi nozzle. *International Journal of Heat and Mass Transfer*, *136*, 1127–1138.

https://doi.org/10.1016/j.ijheatmasstransfer.2019.03.040

Li, J., Song, Y., Yin, J., & Wang, D. (2017). Investigation on the effect of geometrical parameters on the performance of a venturi type bubble generator. *Nuclear Engineering and Design*, *325*(September), 90–96. https://doi.org/10.1016/j.nucengdes.2017.10.006

Ligus, G., Zajac, D., Masiukiewicz, M., & Anweiler, S. (2019). A new method of selecting the airlift pump optimum efficiency at low submergence ratios with the use of image analysis. *Energies*, *12*(4). https://doi.org/10.3390/en12040735

Lim, J. Y., Kim, H. S., Park, S. Y., & Kim, J. H. (2019a). The design of an ejector type microbubble generator for aeration tanks. *Membrane and Water Treatment*, *10*(4), 307–311. https://doi.org/10.12989/MWT.2019.10.4.307

Lim, J. Y., Kim, H. S., Park, S. Y., & Kim, J. H. (2019b). Simultaneous nitrification and denitrification by using ejector type microbubble generator in a single reactor. *Environmental Engineering Research*, *25*(2), 252–257. https://doi.org/10.4491/eer.2018.427

Lim, Y. S., Ganesan, P., Varman, M., Hamad, F. A., & Krishnasamy, S. (2021). Effects of microbubble aeration on water quality and growth performance of Litopenaeus vannamei in biofloc system. *Aquacultural Engineering*, *93*, 102159. https://doi.org/10.1016/j.aquaeng.2021.102159

Liu, C., Tanaka, H., Ma, J., Zhang, L., Zhang, J., Huang, X., & Matsuzawa, Y. (2012). Effect of microbubble and its generation process on mixed liquor properties of activated sludge using Shirasu porous glass (SPG) membrane system. *Water Research*, *46*(18), 6051–6058. https://doi.org/10.1016/j.watres.2012.08.032

Liu, C., Tanaka, H., Zhang, J., Zhang, L., Yang, J., Huang, X., & Kubota, N. (2013). Successful application of Shirasu porous glass (SPG) membrane system for microbubble aeration in a biofilm reactor treating synthetic wastewater. *Separation and Purification Technology*, *103*, 53–59. https://doi.org/10.1016/j.seppur.2012.10.023

Lu, J., Jones, O. G., Yan, W., & Corvalan, C. M. (2023). Microbubbles in food technology. *Annual Review of Food Science and Technology*, *14*(1), 495–515. https://doi.org/10.1146/annurev-food-052720-113207

Mawarni, D. I., Juwana, W. E., Catrawedarma, I., Yuana, K. A., Budhijanto, W., Deendarlianto, D., & Indarto, I. (2023). Statistical characterization of bubble breakup flow structures in swirl-type bubble generator systems. *ASEAN Journal of Chemical Engineering*, *23*(1), 62. https://doi.org/10.22146/ajche.78558

Park, S. K., & Yang, H. C. (2017). Experimental investigation on mixed jet and mass transfer characteristics of horizontal aeration process. *International Journal of Heat and Mass Transfer*, *113*, 544–555. https://doi.org/10.1016/j.ijheatmasstransfer.2017.05.120

Sadatomi, M., Kawahara, A., Kano, K., & Ohtomo, A. (2005). Performance of a new micro-bubble generator with a spherical body in a flowing water tube. *Experimental Thermal and Fluid Science*, *29*(5), 615–623. https://doi.org/10.1016/j.expthermflusci.2004.08.006

Sadatomi, M., Kawahara, A., Matsuura, H., & Shikatani, S. (2012). Micro-bubble generation rate and bubble dissolution rate into water by a simple multi-fluid mixer with orifice and porous tube. *Experimental Thermal and Fluid Science*, *41*, 23–30. https://doi.org/10.1016/j.expthermflusci.2012.03.002

Sari, E. N., Fiveriati, A., Rusti, N., Rulianto, J., Bhiqman Susanto, R., & Catrawedarma, I. (2024). *Visual and pressure signal investigations on bubble produced by ejector bubble generator*. E3S Web of Conferences, 483, 03020. https://doi.org/10.1051/e3sconf/202448303020

Seo, H., Aliyu, A. M., & Kim, K. C. (2018). Enhancement of momentum transfer of bubble swarms using an ejector with water injection. *Energy*, *162*, 892–909. https://doi.org/10.1016/j.energy.2018.08.049

Sun, L., Mo, Z., Zhao, L., Liu, H., Guo, X., Ju, X., & Bao, J. (2017). Characteristics and mechanism of bubble breakup in a bubble generator developed for a small TMSR. *Annals of Nuclear Energy*, *109*, 69–81. https://doi.org/10.1016/j.anucene.2017.05.015

Tabei, K., Haruyama, S., Yamaguchi, S., Shirai, H., & Takakusagi, F. (2007). Study of micro bubble generation by a swirl jet. *Journal of Environment and Engineering*, *2*(1), 172–182. https://doi.org/10.1299/jee.2.172

Terasaka, K., Hirabayashi, A., Nishino, T., Fujioka, S., & Kobayashi, D. (2011). Development of microbubble aerator for waste water treatment using aerobic activated sludge. *Chemical Engineering Science*, *66*(14), 3172–3179. https://doi.org/10.1016/j.ces.2011.02.043

Wu, Z. H., Chen, H. B., Dong, Y. M., Mao, H. L., Sun, J. L., Chen, S. F., Craig, V. S. J., & Hu, J. (2008). Cleaning using nanobubbles: Defouling by electrochemical generation of bubbles. *Journal of Colloid and Interface Science*, *328*(1), 10–14. https://doi.org/10.1016/j.jcis.2008.08.064

Xu, Q., Nakajima, M., Ichikawa, S., Nakamura, N., & Shiina, T. (2008). A comparative study of microbubble generation by mechanical agitation and sonication. *Innovative Food Science and Emerging Technologies*, *9*(4), 489–494. https://doi.org/10.1016/j.ifset.2008.03.003

Yin, J., Li, J., Li, H., Liu, W., & Wang, D. (2015). Experimental study on the bubble generation characteristics for an venturi type bubble generator. *International Journal of Heat and Mass Transfer*, *91*, 218–224.

https://doi.org/10.1016/j.ijheatmasstransfer.2015.05.076

Yoon, R. H. (1993). Microbubble flotation. *Minerals Engineering*, *6*(6), 619–630. https://doi.org/10.1016/0892-6875(93)90116-5

Zhang, H., & Tikekar, R. V. (2021). Air microbubble assisted washing of fresh produce: Effect on microbial detachment and inactivation. *Postharvest Biology and Technology*, *181*, 111687. https://doi.org/10.1016/j.postharvbio.2021.111687

Zhao, L., Mo, Z., Sun, L., Xie, G., Liu, H., Du, M., & Tang, J. (2017). A visualized study of the motion of individual bubbles in a venturi-type bubble generator. *Progress in Nuclear Energy*, *97*, 74–89. https://doi.org/10.1016/j.pnucene.2017.01.004

Zhao, L., Sun, L., Mo, Z., Du, M., Huang, J., Bao, J., Tang, J., & Xie, G. (2019). Effects of the divergent angle on bubble transportation in a rectangular Venturi channel and its performance in producing fine bubbles. *International Journal of Multiphase Flow*, *114*, 192–206. https://doi.org/10.1016/j.ijmultiphaseflow.2019.02.003

Zhao, L., Sun, L., Mo, Z., Tang, J., Hu, L., & Bao, J. (2018). An investigation on bubble motion in liquid flowing through a rectangular Venturi channel. *Experimental Thermal and Fluid Science*, *97*, 48–58. https://doi.org/10.1016/j.expthermflusci.2018.04.009